Available online at www.sciencedirect.com
ScienceDirect
Nuclear and Particle Physics Proceedings 00 (2016) 1–4
Nuclear and Particle Physics Proceedings

Generalized Parton Distributions: recent results *

M. Guidal[a,1], for the CLAS collaboration

[a] *Institut de Physique Nucléaire d'Orsay, CNRS-IN2P3, Université Paris-Sud, Université Paris-Saclay, 91406 Orsay, France.*

Abstract

After an introduction to the field of Generalized Parton Distributions, we present the latest Deep Virtual Compton scattering data recently released by the CLAS collaboration. We then show what is learned from them on the partonic 3-dimensional structure or tomography of the proton.

Keywords: QCD, nucleon structure, parton distributions

1. Introduction

In these short proceedings, we focus on the Deep Virtual Compton (DVCS) process and Generalized Parton Distributions (GPDs) in the valence region. The GPDs are the structure functions of the nucleon which are accessed in the hard exclusive lepto-production of a photon (or a meson) on the nucleon: $lN \to l'N'\gamma$ for DVCS. It has been shown [1–4], about 15 years ago, in the framework of QCD (Quantum-ChromoDynamics) that, at sufficiently large squared electron momentum transfer $Q^2 = (e - e')^2$ and small squared proton momentum transfer $t = (p - p')^2$, the process could be factorized between a hard elementary scattering of a photon on a quark of the nucleon and universal structure functions, namely the GPDs, which parametrize through functions of a few variables the complex non-perturbative quark and gluon structure of the nucleon. See Fig. 1-left for an illustration of this factorization for the DVCS case.

In the quark sector, at QCD leading twist, there are eight GPDs: $H, \tilde{H}, E, \tilde{E}, H_T, \tilde{H}_T, E_T, \tilde{E}_T$. In DVCS, due to helicity conservation arguments, only the first four can be accessed at QCD leading twist. They reflect the four independent spin/helicity transitions between the initial and final nucleons/quarks.

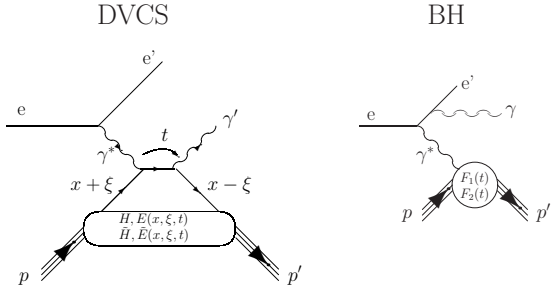

Figure 1: Left: The DVCS process. Right: the BH process.

The GPDs depend on three variables: x, ξ and t (at QCD leading order, which is the framework of the discussion in these proceedings, GPDs don't depend on Q^2). In a frame where the nucleon goes to the speed of light along a certain direction, GPDs represent the probability amplitude of finding a quark in the nucleon with a *longitudinal* momentum fraction $x + \xi$ and of putting it back into the nucleon with a *longitudinal* momentum fraction $x - \xi$, plus some transverse momentum "kick", which is represented by t. It can be shown [5] that t, defined in a momentum space, is the conjugate variable of an impact parameter $b_\perp$, defined in position space. Then, at $\xi = 0$, through a Fourier-like transform, GPDs can also be interpreted as the probability amplitude of

*Talk given at 19th International Conference in Quantum Chromodynamics (QCD 16), 4 - 8 july 2016, Montpellier - FR

finding in a nucleon a parton with a *longitudinal* momentum fraction x at a given *transverse* impact parameter $b_\perp$. One sees then how the information contained in traditional parton distribution functions (PDFs), as measured in inclusive Deep Inelastic Scattering, in which one measures the longitudinal momentum (x) dependence of quarks in the nucleon, and the information contained in form factors (FFs), as measured in elastic lepton-nucleon scattering, which contain the information on the localization ($b_\perp$) of quarks in the nucleon, are now combined and correlated in the GPD description. In the forward limit ($\xi, t \to 0$), GPDs actually reduce to PDFs and their first x-moment are equal to FFs. In addition, the second x-moment of GPDs gives access to the quark angular momentum contribution to the nucleon spin, which is a consequence of this longitudinal momentum-transverse position correlation. We refer the reader to the reviews [6–9] on GPDs for more details on the GPD theoretical formalism.

The way to extract the GPDs from experiment is to measure, at sufficiently large Q^2, the spin-dependent and independent observables of the reaction $lN \to l'N'\gamma$. It is necessary to use beam and target (longitudinal and transverse) polarizations degrees of freedom in order to disentangle the different GPDs. Indeed, each GPD contributes with a different weight according to each individual observable. For instance, on a proton target, the GPD H which describes the distribution of unpolarized quarks in an unpolarized nucleon, contributes mostly to the unpolarized and beam polarized cross sections while the GPD $\tilde{H}$, which describes the distribution of (longitudinally) polarized quarks in a (longitudinally) polarized nucleon, is a major contributor to the spin asymmetries involving a longitudinally polarized target.

Kinematically, the 3-body final state reaction $ep \to ep\gamma$ depends on four independent variables. They are usually chosen as Q^2, x_B, $-t$ and ϕ. x_B is the standard Bjorken variable defined as $\frac{Q^2}{2m_p(E-E')}$ (where E is the beam energy and E' is the scattered electron energy) and is equivalent to ξ. They are related as follows: $\xi = \frac{x_B}{2-x_B}$. ϕ is the azimuthal angle between the electron scattering plane and the hadronic production plane. Among these 4 kinematic variables, only two are thus connected to GPDs (in the QCD leading order approximation where GPDs don't depend on Q^2): ξ and t. This means that the x variable on which GPDs depend as well is not directly measurable. This is due to the loop in the DVCS diagram of Fig. 1-left, which inmplies an integration over x. More precisely, the DVCS amplitude is proportional to: $\int_{-1}^{+1} dx \frac{H(x,\xi,t)}{x-\xi+i\epsilon}$ + ... (where the ellipsis stand for similar terms in E, $\tilde{H}$ and $\tilde{E}$). The $\frac{1}{x-\xi+i\epsilon}$ term is the propagator of the quark between the incoming virtual photon and the outgoing photon. The previous expression can be decomposed into a real and an imaginary part: $PP(\int_{-1}^{+1} dx \frac{H(x,\xi,t)}{x-\xi}) - i\pi H(\xi,\xi,t)$. This means that the maximum information that can be extracted from the experimental data at a given (ξ, t) point is $H(\pm\xi, \xi, t)$, when measuring an observable sensitive to the imaginary part of the DVCS amplitude, and $\int_{-1}^{+1} dx \frac{H(\mp x,\xi,t)}{x\pm\xi}$, when measuring an observable sensitive to the real part of the DVCS amplitude. We will call these two quantities Compton Form Factors (CFFs) in the following. Thus, inevitably, with only DVCS (and DVMP) measurements, a model-dependency is attached to the extraction of the x-dependence of GPDs.

One last experimental concern is that the DVCS process is not the only one contributing to the $ep \to ep\gamma$ reaction. There is also the Bethe-Heitler (BH) process in which the final state photon is radiated by the incoming or scattered electron (see Fig. 1-right) and not by the nucleon itself like in DVCS. It therefore doesn't really contain any new information on the nucleon structure and the GPDs. The BH, which is rather precisely calculable, shall thus be taken into account, at the amplitude level, when extracting GPDs from experiment.

2. The JLab data

The Jefferson Laboratory (JLab), with its $\approx$ 6 GeV intense electron beam, is the facility where DVCS and GPDs are to be studied in the valence region. After a pioneering publication in 2001 of a first DVCS BSA at a single ($< x_B >, < Q^2 >, < t >$)=(0.19, 1.25, -0.19) kinematic point from the CLAS collaboration [10], the Hall A collaboration released in 2006 [11] beam-polarized and unpolarized $ep \to ep\gamma$ cross sections for a few (x_B, Q^2, t) bins. Then, the CLAS collaboration published in 2006 [12] DVCS longitudinally polarized target spin asymmetries (lTSA) for three (x_B, Q^2, t) bins and in 2008 [13] beam spin asymmetries (BSA) for about 60 (x_B, Q^2, t) bins.

This past year, 2015, has seen the release of three new sets of DVCS data from JLab. Regarding CLAS, the collaboration has released lTSAs [14, 15] for 19 (x_B, Q^2, t) bins and beam-polarized and unpolarized $ep \to ep\gamma$ cross sections [16] for $\approx$ 120 (x_B, Q^2, t) bins. Regarding Hall A, the collaboration has published [17] a re-analysis of its earlier data on beam-polarized and unpolarized $ep \to ep\gamma$ cross sections, increasing in passing the number of (x_B, Q^2, t) bins.

Fig. 2 and Fig. 3 show the new CLAS data. Fig. 2 shows 3 particular (out of $\approx$ 120) (x_B, Q^2, t) bins at which the beam-polarized and unpolarized $ep \to ep\gamma$ cross sections were measured as a function of ϕ. The particular shape in ϕ of the unpolarized cross section (green dashed curve in the upper panels of the figure) is due to the BH process. The peaks around $\phi = 0°$ correspond to the cases where the final real photon is emitted along the (initial or scattered) electron's direction, corresponding to a (quasi-)singularity in the process. The difference between the BH curve and the data is the contribution of the DVCS process, i.e. of the GPDs. For the beam-polarized cross sections, a shape close to a $\sin\phi$ is expected, like for the fifth response function $\sigma_{TL'}$ measured in exclusive processes. The amplitude of the sine-like signal stems from the interference between the DVCS and the BH processes. Single polarization observables are in general sensitive to the imaginary part of amplitudes. The BH being purely real, it doesn't produce any polarization asymmetry and this amplitude therefore arises solely from the DVCS contribution.

Fig. 3 shows the 19 (x_B, Q^2, t) bins at which the DVCS lTSA was measured, as a function of ϕ. Like for the BSA, a sine-like form is observed, whose amplitude is a direct (linear) reflection of the DVCS process and of the GPDs.

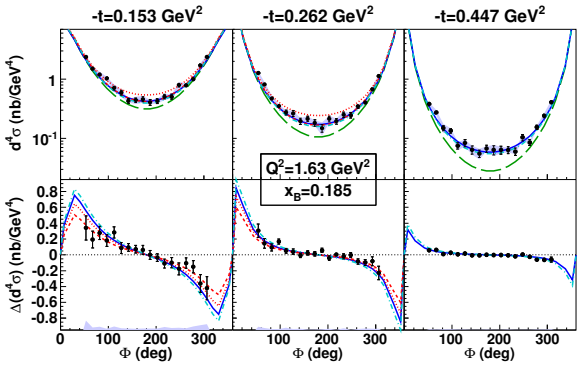

Figure 2: Top: unpolarized $ep \to ep\gamma$ cross section at fixed (x_B, Q^2, t) as a function of ϕ. Bottom: beam-polarized $ep \to ep\gamma$ cross section. Data from Ref. [16]. The green dashed curve corresponds to the BH-only process. The other curves show different GPD models which are described in Ref. [16].

3. From data to a first nucleon imaging

Extracting GPD information from all these DVCS data involve higher-level analysis and specific algorithms. Several fitting techniques have been proposed

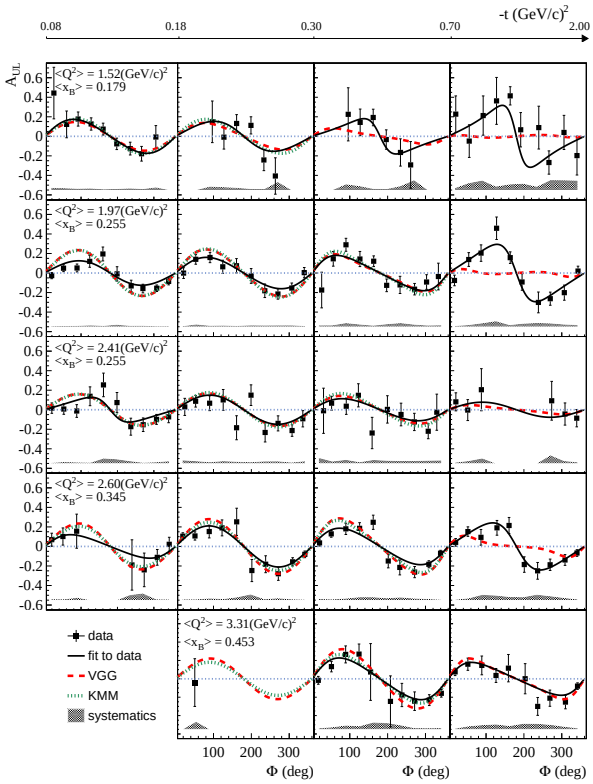

Figure 3: The $ep \to ep\gamma$ longitudinally polarized target spin asymmetries at fixed (x_B, Q^2, t) as a function of ϕ. Data from Refs. [14, 15]. The curves show different GPD models which are described in the previous references.

and developped these past years [18–28] to extract the CFFs from different observables, with more or less model-dependency. In Ref. [29], the latest CLAS and Hall A DVCS data were fitted with the technique of Refs. [18, 23–26] to extract the CFF $\mathcal{H}_{Im}(\xi,t) \equiv H^q(x,\xi,t) - H^q(-x,\xi,t)$. The t-dependence of $\mathcal{H}_{Im}$ for each (ξ,Q^2) bin thus obtained is displayed in Fig. 4. Then, as mentioned earlier, through a Fourier transform and some (small) model-dependent factor, allowing for the transition from the measured $H^q(x,\xi,t) - H^q(-x,\xi,t)$ to $H^q(x,0,t)$, as explained in Ref. [29], one can obtain the x-dependence of the proton transverse charge radius, as displayed in Fig. 5. The increase which is seen of the radius $b_\perp$ as smaller quarks momentum fractions x are probed is a (quasi-)direct reflection of the increase of the t-slope of $\mathcal{H}_{Im}$ as ξ decreases, which can be clearly discerned in Fig. 4. We indeed recall that t is the conjugate variable of $b_\perp$. In passing, the increase of the amplitude of $\mathcal{H}_{Im}$ which can also be clearly distinguished in Fig. 4 reflects the increase of the quark density as

smaller quarks momentum fractions are probed and can be associated to the rise of sea quarks.

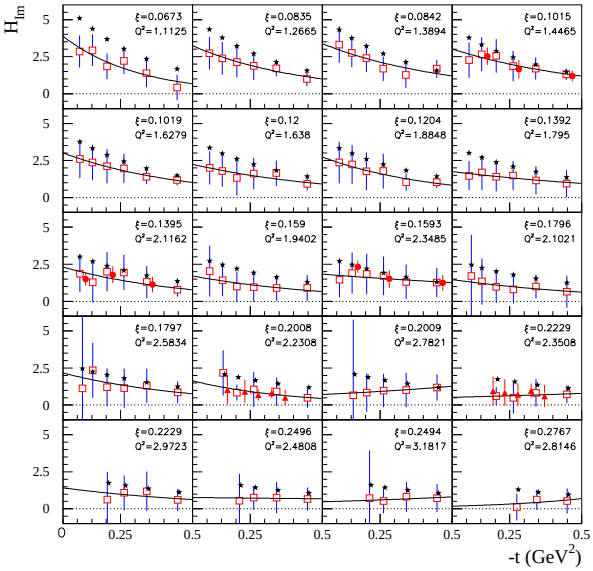

Figure 4: t-dependence of the CFF $\mathcal{H}_{Im}$ for 20 CLAS $(x_B,\ Q^2)$ bins. Open squares: results of the fit to the CLAS beam-polarized and unpolarized $ep \to ep\gamma$ cross sections. Solid circles: results of the fit to the same CLAS data with the CLAS lTSA in addition. Solid triangles: results of fit to the Hall A beam-polarized and unpolarized $ep \to ep\gamma$ cross sections. Other symbols and curves explained in Ref. [29].

4. Conclusion

In these proceedings, we have given a very brief overview of the GPD physics and we have presented some of the latetst DVCS data issued from JLab and in particular from the CLAS collaboration. We then showed the extraction of the CFF $\mathcal{H}_{Im}$ according to a particular method, from which the x-dependence of the proton charged radius could be derived. Several new experiments are planned to measure new observables and new data expected over a broader phase space in the coming years with the 12 GeV beam energy at JLab. This promises important new advances in the field of nucleon structure.

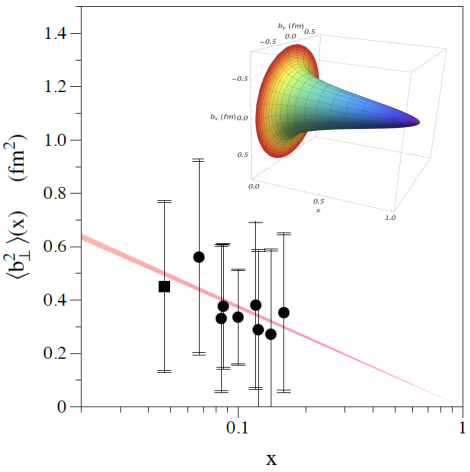

Figure 5: x-dependence of the proton charge radius according to the analysis of Ref. [29]. The inset is an extension beyond the data range based on a fit. See the reference for details.

References

[1] D. Muüller, D. Robaschik, B. Geyer, F. M. Dittes and J. Horejsi, Fortsch. Phys. **42**, 101 (1994).
[2] X. Ji, Phys. Rev. Lett. **78**, 610 (1997).
[3] A.V. Radyushkin, Phys. Lett. B **380**, 417 (1996).
[4] X. Ji, Phys. Rev. D **55**, 7114 (1997).
[5] M. Burkardt, Phys. Rev. D **62**, 071503 (2000).
[6] K. Goeke, M. V. Polyakov and M. Vanderhaeghen, Prog. Part. Nucl. Phys. **47**, 401 (2001).
[7] M. Diehl, Phys. Rept. **388**, 41 (2003).
[8] A.V. Belitsky, A.V. Radyushkin, *Phys. Rept.* **418**, 1 (2005).
[9] M. Guidal, H. Moutarde and M. Vanderhaeghen, Rept. Prog. Phys. **76**, 066202 (2013).
[10] S. Stepanyan et al., Phys. Rev. Lett. **87**, 182002 (2001).
[11] C. Muñoz Camacho *et al.*, Phys. Rev. Lett. **97**, 262002 (2006).
[12] S. Chen *et al.*, *Phys. Rev. Lett.* **97**, 072002 (2006).
[13] F.-X. Girod *et al.*, *Phys. Rev. Lett.* **100**, 162002 (2008).
[14] E. Seder *et al.* [CLAS Coll.], Phys. Rev. Lett. **114** 3, 032001 (2015) [Phys. Rev. Lett. **114** 8, 089901 (2015)].
[15] S. Pisano *et al.* [CLAS Coll.], Phys. Rev. D **91** 5, 052014 (2015).
[16] H. S. Jo *et al.* [CLAS Coll.], Phys. Rev. Lett. **115**, 212003 (2015).
[17] M. Defurne *et al.* [Jefferson Lab Hall A Coll.], Phys. Rev. C **92** 5, 055202 (2015).
[18] M. Guidal, Eur. Phys. J. A **37**, 319 (2008). [Erratum-ibid. A **40**, 119 (2009)]
[19] K.Kumericki and D. Müller, Nucl. Phys. B **841**, 1 (2010).
[20] K. Kumericki, D. Müller and M. Murray, Nuovo Cim. C **036** (2013) no.05, 159
[21] K. Kumericki, D. Müller and M. Murray, Phys. Part. Nucl. **45** (2014) no.4, 723
[22] H. Moutarde, Phys. Rev. D **79**, 094021 (2009).
[23] M. Guidal and H. Moutarde, Eur. Phys. J. A **42**, 71 (2009).
[24] M. Guidal, Phys. Lett. B **689**, 156 (2010).
[25] M. Guidal, Phys. Lett. B **693**, 17 (2010).
[26] M. Boër and M. Guidal, J. Phys. G **42** (2015) no.3, 034023 doi:10.1088/0954-3899/42/3/034023
[27] K. Kumericki and D. Muüller, Int. J. Mod. Phys. Conf. Ser. **40** (2016) 1660047.
[28] K. Kumericki, S. Liuti and H. Moutarde, Eur. Phys. J. A **52** (2016) no.6, 157
[29] R. Dupré, M. Guidal and M. Vanderhaeghen, arXiv:1606.07821 [hep-ph].